International Journal of Ambient Energy

ISSN: (Print) (Online) Journal homepage: https://www.tandfonline.com/loi/taen20

# Electroosmosis and transverse magnetic effects on radiative tangent hyperbolic nanofluid flow through porous medium

K. Ramesh , Aryaman Patel & Madhav Rawal

**To cite this article:** K. Ramesh , Aryaman Patel & Madhav Rawal (2021): Electroosmosis and transverse magnetic effects on radiative tangent hyperbolic nanofluid flow through porous medium, International Journal of Ambient Energy, DOI: 10.1080/01430750.2020.1862912

**To link to this article:** https://doi.org/10.1080/01430750.2020.1862912

Published online: 04 Jan 2021.

INTERNATIONAL JOURNAL OF AMBIENT ENERGY
https://doi.org/10.1080/01430750.2020.1862912

Taylor & Francis
Taylor & Francis Group



# Electroosmosis and transverse magnetic effects on radiative tangent hyperbolic nanofluid flow through porous medium

K. Ramesh [a], Aryaman Patel[b] and Madhav Rawal[b]

[a]Department of Mathematics, Symbiosis Institute of Technology, Symbiosis International (Deemed University), Pune, India; [b]Department of Mechanical Engineering, Symbiosis Institute of Technology, Symbiosis International (Deemed University), Pune, India

**ABSTRACT**

Modelling the thermal and fluid properties based on fluid dynamic theory helps us better understand its mechanism and the effects of the flow conditions on the fluid. These concepts find their applications in understanding drug delivery, heat regulations in industrial machinery and military applications. In this study, the effect of MHD and electroosmosis on the radiative tangent hyperbolic nanofluid flow through a porous medium is investigated. Darcy's law, Brownian motion and thermophoresis effects have also been taken into consideration. In the process of formulation, the set of non-linear differential equations have been obtained. The equations for the continuity, momentum, temperature and nanoparticle volume fraction have been modified under the suitable non-dimensional quantities. The resulting dimensionless system of the equations have been solved using the bvp4c package in MATLAB software. It is observed that the velocity of the fluid increases with an increase in electroosmotic parameter. The velocity of the fluid increases with the increment in Darcy number. The temperature of the fluid significantly decreases with an increase in radiation parameter. The effects of Brownian motion and thermophoresis parameters on the nanoparticle volume fraction show that the nanoparticle volume fraction increases with the increment in Brownian motion parameter and significant decrement with the increase of thermophoresis parameter. Furthermore, the comparison study has been established in the presence/absence of electroosmosis parameter on the flow of Newtonian and tangent hyperbolic nanofluids.

**ARTICLE HISTORY**
Received 26 August 2020
Accepted 1 December 2020

**KEYWORDS**
Tangent hyperbolic nanofluid; thermofluid dynamics; magnetofluid dynamics; electroosmosis; hall currents

## Nomenclature

| | |
|---|---|
| $u$: | Velocity component ($m \cdot s^{-1}$) |
| $t$: | Time (s) |
| $\rho_f$: | Density of the fluid ($kg \cdot m^{-3}$) |
| $\rho_p$: | Density of the nanoparticles ($kg \cdot m^{-3}$) |
| $B_0$: | Magnetic field (T) |
| $\bar{p}$: | Pressure (Pa) |
| $x$: | Axial coordinate (m) |
| $y$: | Transverse coordinate (m) |
| $k_f$: | Thermal conductivity ($W \cdot m^{-1} \cdot K^{-1}$) |
| $E_x$: | Axial electric field ($m \cdot kg \cdot s^3 \cdot A^1$) |
| $l$: | Characteristic length (m) |
| $\bar{\phi}$: | Electric potential (V) |
| $\xi_1, \xi_2$: | Zeta potentials (V) |
| $m$: | Hall current ($m^3 \cdot C^{-1}$) |
| $\mu_f$: | Viscosity ($kg \cdot m^{-1} \cdot s^{-1}$) |
| $P_e$: | Electron pressure (Pa) |
| $e$: | Electrical charge (C) |
| $\bar{\tau}$: | Stress tensor |
| $\Gamma$: | Material constant |
| $n$: | Power law index |
| $\bar{\dot{r}}$: | Shear rate tensor |
| $\bar{J}$: | Current vector |
| $\mu_0$: | Zero shear rate viscosity |
| $\mu_\infty$: | Infinite shear rate viscosity |
| $\omega_e$: | Cyclotron frequency |
| $\mu_e$: | Magnetic permeability |
| $n_0$: | Bulk concentration |
| $T_m$: | Mean fluid temperature |
| $\theta$: | Dimensionless nanoparticle temperature |
| $\sigma$: | Dimensionless nanoparticle volume fraction |
| $M$: | Hartmann Number |
| $Da$: | Darcy Number |
| $G$: | Pressure Gradient |
| $\kappa$: | Electroosmotic parameter |
| $Nt$: | Thermophoresis parameter |
| $Nb$: | Brownian parameter |
| $Rn$: | Radiation parameter |
| $Pr$: | Prandtl number |
| $\epsilon$: | Dielectric permittivity |
| $U_{HS}$: | Helmholtz–Smoluchowski velocity |
| $D_B$: | Brownian diffusion coefficient |
| $D_T$: | Thermophoresis diffusion coefficient |
| $We$: | Weissenberg number |
| $\tau_e$: | Electron collision time |
| $k_B$: | Boltzmann constant |
| $z$: | Valence of ions |

**CONTACT** K. Ramesh ramesh.katta1@gmail.com

## 1. Introduction

Nanofluids are nanotechnology-based fluids with dispersed and stably suspended nanosized particles that facilitated the development of a novel class of heat transfer fluids with an enhanced thermal conductivity, thermal diffusivity and viscosity (Choi and Eastman 1995). Traditionally the size of the suspended nanoparticles is between 1 and 100 nm. They have been increasingly used in industrial cooling applications, nuclear reactors, microelectrochemical systems and cryopreservation, due to their low-cost operation and higher energy efficiency and better performance. Whenever the small solid elements can added to fluids then there will be significant improvement in the heat conductivity of nanofluids (Das et al. 2007). Lee et al. (1999) have investigated the thermal conductivity enhancement of nanofluids to the scientific community. Keblinski, Eastman, and Cahill (2005) have observed that for the possibility of clustered nanoparticles into small aggregates, nanoparticles occupy more space than the individual nanoparticles that make up the aggregates, resulting in a larger volume fraction and hence, enhanced thermal conductivity. Kim et al. (2007) have conducted a study of pool boiling and heat flux enhancement of nanofluids. They have studied the pool boiling characteristics of nanofluid with alumina, zirconia and silica as the nanoparticles dispersed in water as the base fluid. Sheikholeslami et al. (2015) have presented the numerical investigation on the effects of radiation on the MHD nanofluid flow between two horizontal rotating plates. Zhang et al. (2015) have investigated the heat transfer of MHD nanofluids of different nanoparticles (aluminium oxide, silver and copper) with the effects of variable surface heat flux and first-order chemical reaction against a flat plate in porous medium. Shafiq, Jabeen, et al. (2017) have modelled the flow of a nanofluid incorporating the heat transfer model under the squeeze flow effect. Naseem et al. (2018) have used the optimal homotopy technique to solve the non-linear set of equations incorporating the heat and mass flux model on a riga plate under the various effects on the nanofluid. Shafiq, Hammouch, and Turab (2018) have studied the stagnation point propulsion of a nanofluid induced by a riga plate. The series of studies (Ganesh, Chamkha, et al. 2018; Ganesh, Kameswaran, et al. 2018; Ganesh, Al-Mdallal, and Kameswaran 2019) have focussed on the alumina-based nanoparticles along with different base fluids and under various flow and boundary conditions. Sharma et al. (2019) have investigated the combined effects of electric field and peristaltic pumping on the nanofluid flow through the microchannel. Shafiq, Khan, et al. (2020) have analysed the effect of electromagnetic forces on the two distinct types of carbon nanotubes (single and multi-walled) with water as the base solvent. Some more recent investigations can be observed in the current direction through Shafiq and Sindhu (2017); Naseem et al. (2018); Ganesh, Al-Mdallal, et al. (2019); Rasool et al. (2020); Shafiq, Zari, et al. (2020), and the references therein.

The movement of fluid induced due to the presence of an electric field through porous medium or semipermeable membrane is electro-osmosis. This was first discovered by Porrett in 1816 wherein he used a medicine phial with a moistened bladder interposed between them (as the membrane), after filling the two cells with unequal amounts of electrolytic fluid and applying electric potential to the two sides, he noticed that the fluid obeys the impulse of the voltaic current from positive to negative hence, levelling the fluid on both the sides of the phial. This intuitive behaviour is due to the fact that the interface between the electrolyte and the container wall generally forms a double layer named Debye layer. This double layer has a small voltage across it, called as zeta potential defined as the difference of the potential of surface and the potential just outside the double layer. When the electric field is applied across this surface then it produces an effective slip velocity outside the double layer by dragging the fluid. Hence, causes the electro-osmotic flow. Electro-osmosis has its applications in microfluidics, soil analysis and chemical analysis. Fensom and Dainty (1963) have successfully recorded the electro-osmotic transport of the order of 100 moles of water per faraday in the direction of positive ion flow when they passed water and electric current through a single cell of Nitella translucens. Shapiro and Probstein (1993) have investigated the application of electroosmosis in removal of contaminants from saturated clay. They have experimented by preparing a kaolinite sample loaded with a known amount of acetic acid and phenol. They found that the process effectively of up to 94% in the removal of these species from the clay. Jiang et al. (2002) have developed a compact cooling system technology using closed loop two-phase microchannel system that uses electro-osmotic pumping for cooling of VLSI (Very-Large Scale Integration) circuits. They have also noticed that the rate of flow can easily be controlled by controlling the electric field. Patel and Kassegne (2007) have discussed the electroosmosis and thermal effects in MHD micropumps using finite difference method. They have observed that transverse electro-osmotic flow had considerable effects on the efficiency of the pumps along with noticeable increase in conductivity of electrolyte with Joule heating.

A skeletal material containing interconnected network of pores or voids are called as porous materials (Liu and Ma 2006; Liu and Chen 2014). The pores are usually filled with fluids (gaseous or liquid). The properties of these materials depend on porosity, which is the ratio of pore volume to the whole nominal volume of the porous material (Nield and Bejan 1999). This basic parameter helps in the determination of properties like thermal and electrical conductivity, optical properties, filtration and tensile strength. Darcy (1856) through his investigation and experiments on steady state, unidirectional flow over a uniform medium concluded that discharge rate is proportional to the pressure drop and viscosity of the fluid through the specific distance. This law explains the dependencies of fluid flow through porous materials (Mahdi et al. 2015). Porous materials also find their applications for the development of gas sensors and separators. Porous materials deform significantly at relatively low stresses which is useful to prevent heavy damages to spacecrafts after possible impact of space debris. Li, Li, and Zhang (2004) have found that tiny porous silicon carbide balls have a better energy absorption property and are suitable to resist high energy hypervelocity impact. Bakier (2001) presented the effect of radiation parameter on forced convection from a flat plate in different orientations in a saturated permeable medium. Zahmatkesh (2007) have discussed the development of free convective flow due to the influence of thermal radiation with porous medium. Shafiq, Rasool, and Khalique (2020) have studied the effect of thermal slip and convection on the nanofluid flows through a porous medium. Alfven (1942) was the first to bring

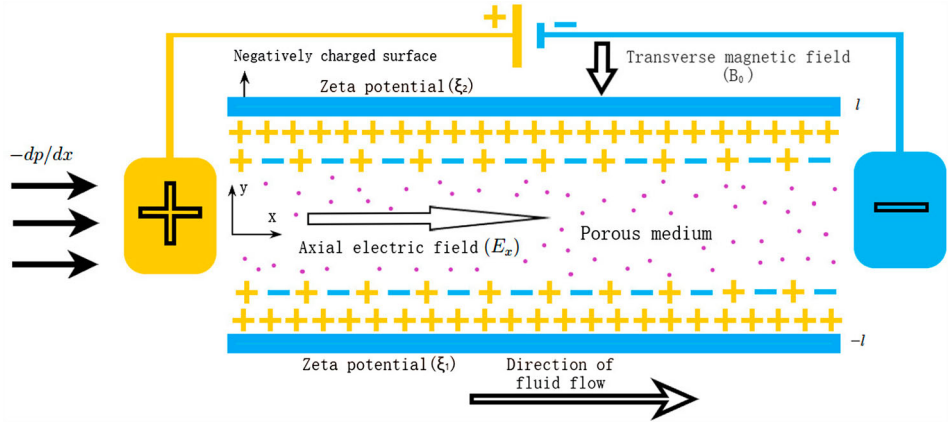


**Figure 1.** Geometry of the current problem.

the attention towards the characteristics of a conducting fluid in motion under the effects of unvarying magnetic field, this resulted in the polarisation of the conductive fluid and in turn change in the magnetic field. This found its immediate application in solar physics as sun has a magnetic field and plasma is a conducting fluid. The combination set of Navier–Stokes equation and Maxwell's equation gave the mathematical formulation for the magnetohydrodynamics. Many authors have focussed their attention on the MHD in different fluid flow problems. Shafiq, Hammouch, and Sindhu (2017) have studied the bioconvection and MHD effect on the flow model of a tangent hyperbolic nanofluid. Rasool, Zhang, et al. (2019) have investigated the entropy generation on the nanofluid flow under the MHD and porous medium. Few more research articles (Rasool, Shafiq, et al. 2019; Shafiq, Khan, et al. 2019; Shafiq, Zari, et al. 2019) can be seen in this direction.

Tangent hyperbolic fluid is one of the interesting model among the aforementioned non-Newtonian fluid models, which is developed for chemical engineering systems. This model has many advantages as compared with other non-Newtonian fluids such as simplicity, ease of computation and physical robustness. Moreover, it is reduced from the liquid's kinetic energy rather than the empirical relation. Many scientific works have been made based on the tangent hyperbolic fluid model. As per the authors knowledge, no work has yet been done on the study of tangent hyperbolic nanofluid flow in a microchannel under the effects of MHD, Hall current, electroosmosis and porous medium. To fill this literature gap, the current article focuses to study the influences of the Hall effect, MHD and electroosmosis on the flow of tangent hyperbolic nanofluid in a microchannel. The non-dimensional system of equations have been solved using the bvp4c method in MATLAB. The mathematical formulation has been discussed in the next section, followed by the results and discussion of the graphical representation. The last section describes the important outcomes of the study.

## 2. Mathematical formulation

Consider the flow of tangent hyperbolic nanofluid in the presence of magnetic field and electroosmosis. The flow is considered along the $x$-direction, between two plates under constant pressure and electroosmosis. A uniform magnetic field of strength $B_0$ is applied in the direction perpendicular to the flow. The lower wall is maintained at temperature $T_0$, concentration at $C_0$ and the upper wall is maintained at temperature $T_1$ and concentration $C_1$ respectively (see Figure 1). It is also assumed that the choice of velocity chosen as $(u(y), 0, 0)$. The mathematical model (continuity, momentum, energy and nanoparticle volume fraction) for the MHD tangent hyperbolic nanofluid under the electroosmosis and porous medium may be put in the form:

$$\nabla.\bar{q} = 0, \tag{1}$$

$$\rho_f\left(\frac{\partial \bar{q}}{\partial t} + (\bar{q}.\nabla)\bar{q}\right) = -\nabla\bar{p} + \nabla.\bar{\tau} + \bar{R} + \bar{J}\times\bar{B} + \rho_e E_x, \tag{2}$$

$$(\rho c)_f\left(\frac{\partial T}{\partial t} + (\bar{q}.\nabla)T\right) = k_f\nabla^2 T - \nabla.q_r + (\rho c)_p D_B \nabla T.\nabla C + (\rho c)_p \frac{D_T}{T_m}\nabla T.\nabla T, \tag{3}$$

$$\left(\frac{\partial C}{\partial t} + (\bar{q}.\nabla)C\right) = D_B\nabla^2 C + \frac{D_T}{T_m}\nabla^2 T. \tag{4}$$

The extra stress tensor for the tangent hyperbolic nanofluid can be written as

$$\bar{\tau} = (\mu_\infty + (\mu_f + \mu_\infty)\tanh(\Gamma\bar{\dot{r}})^n)\bar{A}, \tag{5}$$

in which $\mu_f$ is the zero-shear rate viscosity, $\mu_\infty$ is the infinite shear rate viscosity, $\Gamma$ is the material constant, $n$ is the power law index and $\bar{\dot{r}}(=\sqrt{\Pi/2})$ (here $\Pi = \bar{A}^2/2$ and $\bar{A} = \nabla\bar{q} + (\nabla\bar{q})^{\mathrm{T}}$) is the shear rate tensor. Let us consider $\mu_\infty = 0$ and $\Gamma\bar{\dot{r}} < 1$, under these considerations and the choice of velocity, the extra stress tensor is given by

$$\bar{\tau} = \mu_f\left((1-n)\frac{du}{dy} + \frac{n\Gamma}{\sqrt{2}}\left(\frac{du}{dy}\right)^2\right). \tag{6}$$

The current vector can be written as

$$\bar{J} = \sigma\left(\bar{E} + \bar{q}\times\bar{B}\right). \tag{7}$$

In the above equation, electric conductivity is known as $\sigma$ and electric field corresponds to $\bar{E}$. The thermoelectric effects, polarisation effects and external electric field effects are considered

zero. In view of these considerations, we get

$$\bar{J} \times \bar{B} = \left( \frac{-\sigma B_o^2 u}{1+m^2}, 0, 0 \right). \tag{8}$$

Using concept of Darcy's law, the pressure drop and velocity can be related through the equation

$$\nabla \bar{p} = \frac{-\mu_f \phi_1}{k} \bar{q}, \tag{9}$$

under the mentioned choice of velocity, one can get

$$\bar{R} = \left( \frac{-\mu_f \phi_1 u}{k}, 0, 0 \right). \tag{10}$$

The well-known Poisson's equation may be of the form:

$$\nabla^2 \bar{\phi} = \frac{-\bar{\rho_e}}{\epsilon}. \tag{11}$$

Here, electric potential is given by $\bar{\phi}$, the dielectric permittivity is given by $\epsilon$ and $\bar{\rho_e} = (-2n_o e^2 z^2 \bar{\phi}/k_B T_v)$ (under the Taylor's series $((|ez\bar{\phi}/k_B T_v| < 1))$ approximations) is the Boltzmann distribution is followed by charge distribution, where $n_o$ is the bulk concentration, $T_v$ is the average temperature, $z$ is the valence of ions, $e$ is the elementary charge valence and $k_B$ is the Boltzmann constant. Under the aforementioned theory, the Poisson's equation (11) can be written as

$$\nabla^2 \bar{\phi} = \left( \frac{-2n_o e^2 z^2 \bar{\phi}}{k_B T_v \epsilon} \right). \tag{12}$$

Using the above-mentioned theories and approximations, the momentum, energy and nanoparticle volume fraction equation can be written as

$$\mu_f (1-n) \frac{\mathrm{d}^2 \bar{u}}{\mathrm{d}\bar{y}^2} + \sqrt{2} \Gamma n \mu_f \frac{\mathrm{d}\bar{u}}{\mathrm{d}\bar{y}} \frac{\mathrm{d}^2 \bar{u}}{\mathrm{d}\bar{y}^2} - \left( \frac{\sigma B_o^2}{1+m^2} + \frac{\mu_f \phi}{k} \right) \bar{u} - \left( \frac{2n_o e^2 z^2 \bar{\phi}}{k_B T_v \epsilon} \right) E_x + G = 0, \tag{13}$$

$$k_f \left( \frac{\mathrm{d}^2 \bar{T}}{\mathrm{d}\bar{y}^2} \right) + (\rho c)_p D_B \left( \frac{\mathrm{d}\bar{C}}{\mathrm{d}\bar{y}} \frac{\mathrm{d}\bar{T}}{\mathrm{d}\bar{y}} \right) + \frac{(\rho c)_p D_T}{T_m} \left( \frac{\mathrm{d}\bar{T}}{\mathrm{d}\bar{y}} \right)^2 + \frac{16\sigma^* T_0^3}{3\alpha^*} \frac{\mathrm{d}^2 \bar{T}}{\mathrm{d}\bar{y}^2} = 0, \tag{14}$$

$$D_B \left( \frac{\mathrm{d}^2 \bar{C}}{\mathrm{d}\bar{y}^2} \right) + \frac{D_T}{T_m} \left( \frac{\mathrm{d}^2 \bar{T}}{\mathrm{d}\bar{y}^2} \right) = 0, \tag{15}$$

with the corresponding boundary conditions

$$\bar{u} = 0, \quad \bar{T} = T_0, \quad \bar{C} = C_0 \quad \text{at } \bar{y} = -l, \tag{16}$$

$$\bar{u} = U, \quad \bar{T} = T_1, \quad \bar{C} = C_1 \quad \text{at } \bar{y} = l. \tag{17}$$

Consider the following non-dimensional quantities:

$$u = \frac{\bar{u}}{U}, \quad y = \frac{\bar{y}}{l}, \quad G = \frac{l^2 \bar{G}}{\mu_f U}, \quad M = \sqrt{\frac{\sigma}{\mu_f}} B_0 l,$$

$$D_a = \frac{k}{\phi l^2}, \quad \phi = \frac{\bar{\phi}}{\xi}, \quad , W_e = \frac{\Gamma U}{l},$$

$$U_{HS} = \frac{-E_x \epsilon \xi}{\mu_f U}, \quad \kappa = lez \sqrt{\frac{2n_o}{k_B T_v \epsilon}}, \quad \tau = \frac{(\rho c)_p}{(\rho c)_f},$$

$$\theta = \frac{\bar{T} - T_0}{T_1 - T_0}, \quad \sigma = \frac{\bar{C} - C_0}{C_1 - C_0},$$

$$Nb = \frac{\rho_f \tau D_B (C_1 - C_0)}{\mu_f}, \quad Nt = \frac{\rho_f \tau D_T (T_1 - T_0)}{T_m \mu_f},$$

$$Pr = \frac{\mu c_f}{k_f}, \quad Rn = \frac{16\sigma^* T_0^3}{3\mu_f \alpha^* c_f}.$$

Considering these non-dimensional quantities, Equation (12) can be written as

$$\frac{\mathrm{d}^2 \phi}{\mathrm{d}y^2} - \kappa^2 \phi = 0. \tag{18}$$

Under the non-dimensional conditions $\phi = \xi_1$ at $y = -1$ and $\phi = \xi_2$ at $y = 1$, the resulting electric potential can be obtained as

$$\phi = \left( \frac{\xi_1 + \xi_2}{2\cosh(\kappa)} \right) (\cosh(\kappa y)) - \left( \frac{\xi_1 - \xi_2}{2\sinh(\kappa)} \right) (\sinh(\kappa y)). \tag{19}$$

Under the aforementioned assumptions and dimensionless quantities, the resulting non-dimensional governing equations can be put in the form

$$\left( (1-n) \frac{\mathrm{d}^2 u}{\mathrm{d}y^2} + \sqrt{2} n W_e \frac{\mathrm{d}u}{\mathrm{d}y} \frac{\mathrm{d}^2 u}{\mathrm{d}y^2} \right) - \left( \frac{M^2}{1+m^2} + \frac{1}{Da} \right) u + \kappa^2 U_{HS} \phi + G = 0, \tag{20}$$

$$\frac{\mathrm{d}^2 \theta}{\mathrm{d}y^2} + NbPr \left( \frac{\mathrm{d}\sigma}{\mathrm{d}y} \frac{\mathrm{d}\theta}{\mathrm{d}y} \right) + NtPr \left( \frac{\mathrm{d}\theta}{\mathrm{d}y} \right)^2 + RnPr \frac{\mathrm{d}^2 \theta}{\mathrm{d}y^2} = 0, \tag{21}$$

$$\frac{\mathrm{d}^2 \sigma}{\mathrm{d}y^2} + \frac{Nt}{Nb} \frac{\mathrm{d}^2 \theta}{\mathrm{d}y^2} = 0, \tag{22}$$

with the non-dimensional boundary conditions

$$u = 0, \quad \theta = 0, \quad \sigma = 0 \quad \text{at } y = -1, \tag{23}$$

$$u = 1, \quad \theta = 1, \quad \sigma = 1 \quad \text{at } y = 1. \tag{24}$$

## 3. Results and discussion

The system of equations from (20) to (22) are highly nonlinear, therefore, it is not possible to solve them analytically. To solve equations (20)–(22) with the conditions (23)–(24), we have used bvp4c technique through MATLAB software. Table 1 represents the comparison of velocity between the current study and the existing literature (Ramesh 2018). It is depicted from this table

**Table 1.** Comparison of velocity profile of existing literature (in case of $\beta = 0, \lambda_1 = 0$) (Ramesh 2018) and present investigation (in case of $m = 0, n = 0, \kappa = 0$).

| $y$ | Ramesh (2018) | Current study | Error |
|---|---|---|---|
| −1 | 0.000000000 | 0.000000000 | 0.0000000E+00 |
| −0.8 | 0.038488401 | 0.038487855 | 5.4599732E−07 |
| −0.6 | 0.057653241 | 0.057652938 | 3.0240260E−07 |
| −0.4 | 0.068737112 | 0.068737340 | 2.2793944E−07 |
| −0.2 | 0.078242103 | 0.078243085 | 9.8267280E−07 |
| 0 | 0.091744088 | 0.091746173 | 2.0842652E−06 |
| 0.2 | 0.117163686 | 0.117167410 | 3.7239776E−06 |
| 0.4 | 0.169412694 | 0.169418701 | 6.0071865E−06 |
| 0.6 | 0.279141742 | 0.279150255 | 8.5127708E−06 |
| 0.8 | 0.51072075 | 0.510729764 | 9.0133689E−06 |
| 1 | 1.000000000 | 1.000000000 | 0.0000000E+00 |

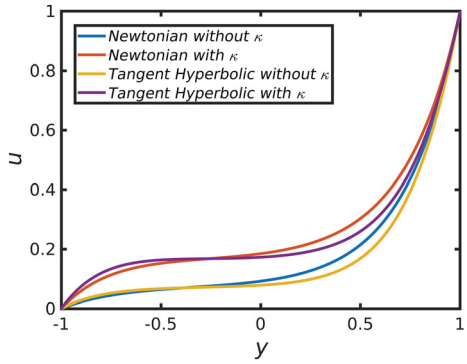


**Figure 2.** Velocity profiles for Newtonian and tangent hyperbolic nanofluids with/without electroosmosis effects.

that the current results are in good agreement with the existing literature. For the comparison, it is assumed the involved parameters as $M = 2$, $Da = 0.1$ and $G = 1$. Figure 2 is provided to see the behaviour of velocity for the Newtonian and tangent hyperbolic nanofluid models with/without electroosmosis effects. It is noted from this figure that, in both the cases the maximum velocities are seen in the presence of electroosmosis effects and the minimum velocities are noticed in the absence of electroosmosis effects.

Figure 3 deals with the effects of Darcy number *Da*, pressure gradient *G*, Hall current parameter *m* and Hartmann number *M* on the velocity of the nanofluid. It is noticed from Figure 3(a) that the velocity decreases with rising values of Hartmann number. Hartmann number gives the relation between electromagnetic force and the viscous force. The magnetic force acts along the perpendicular direction to the fluid flow therefore, as the Hartmann number increases the Lorentz force also increases; this increment causes the hindrance in the fluid flow. Darcy's law computes the flow of the fluid through a porous medium, as the permeability increases the fluid velocity increases and hence with the higher values of Darcy number, the velocity increases (see Figure 3(b)). From Figure 3(c), it is clear that the pressure gradient *G* increases the fluid velocity increases. It is physically signifies, whenever we apply more pressure to the flow, there should be more fluid takes place in the system. Due to this reason, the velocity of the nanofluid increases as the pressure gradient increases. Figure 3(d) shows that as the Hall current *m* increases, the velocity of the nanofluid increases.

Figure 4 is prepared to see the effects of thermophoresis parameter *Nt*, Brownian motion parameter *Nb*, Prandtl number *Pr* and radiation parameter *Rn* on the nanoparticle temperature of the nanofluid. Increase in Brownian motion increases the random motion of the nanoparticles. This increment in random movement causes the particles to gain energy and hence there will be a rise in temperature with the increment in Brownian motion parameter *Nb*. For this reason, the increase effect in the nanoparticle temperature is observed with respect to Brownian motion parameter (see Figure 4(a)). Figure 4(b) shows an increment in nanoparticle temperature with increase in thermophoresis parameter *Nt*. This is because thermophoresis parameter is directly affected by thermophoresis diffusion coefficient, this enhances the movement of the nanofluid and the particles gain kinetic energy resulting in an increase in nanoparticle temperature of the nanofluid. Prandtl number *Pr* gives the

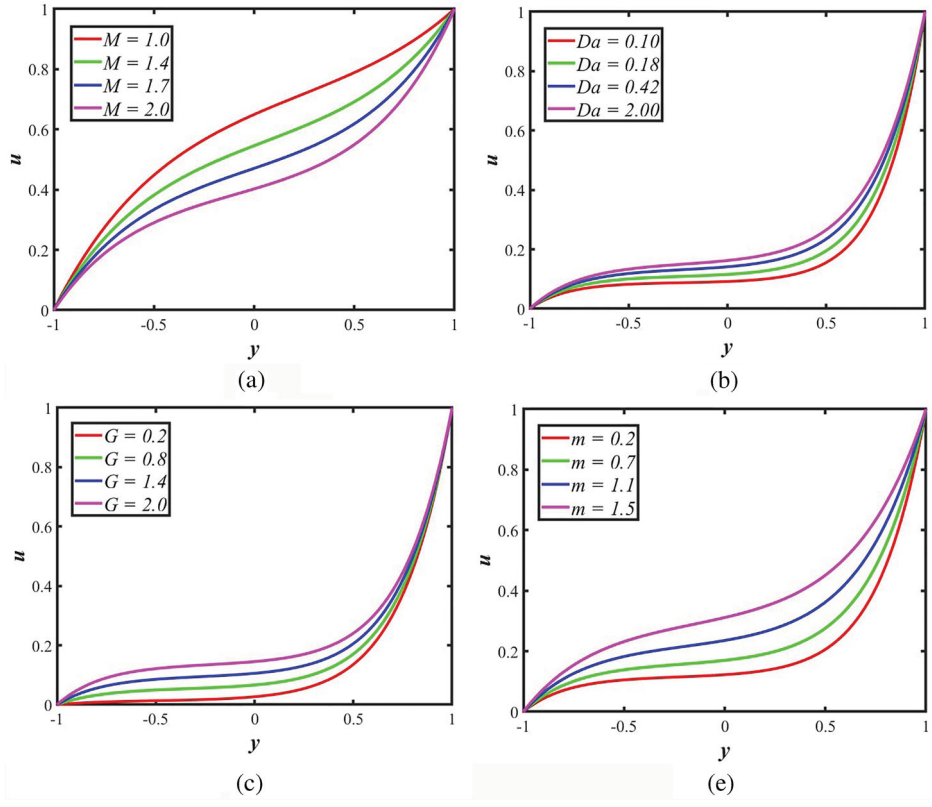


**Figure 3.** Variations in velocity for various fluid flow parameters.

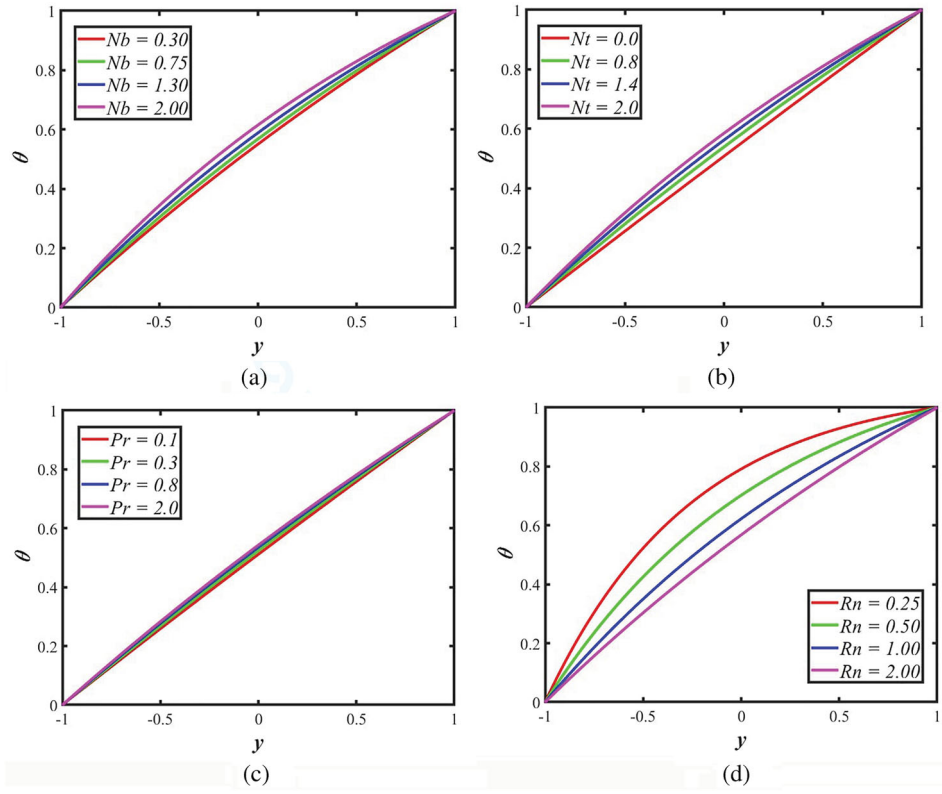


**Figure 4.** Variations in temperature for various fluid flow parameters.

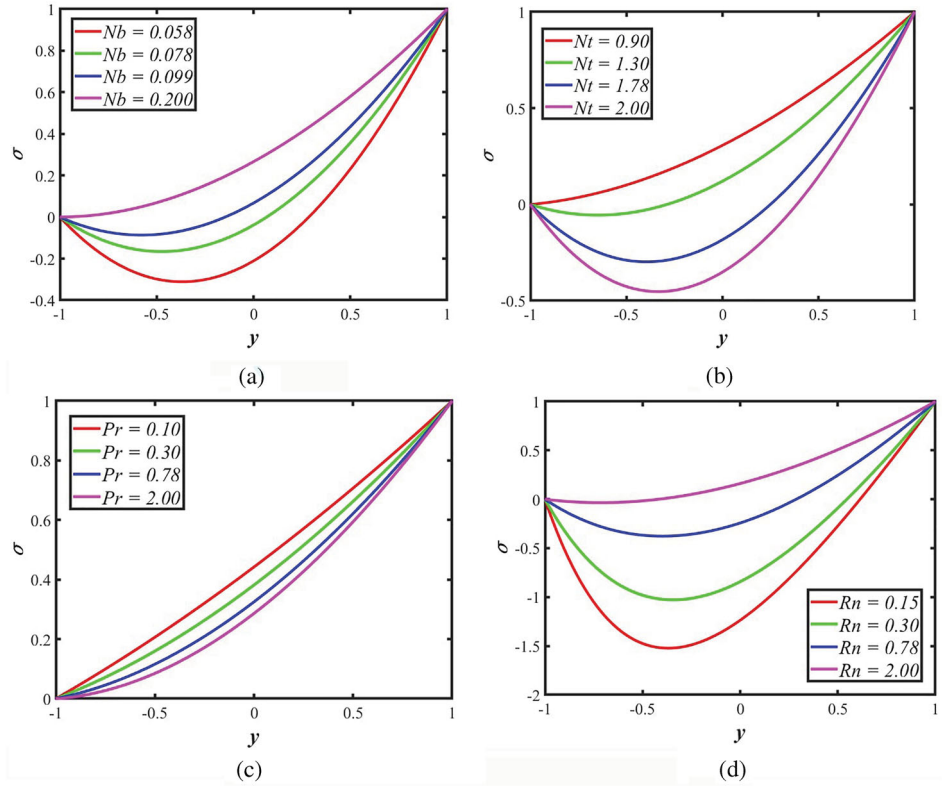


**Figure 5.** Variations in nanoparticle volume fraction for various fluid flow parameters.

relation between thermal conductivity and viscosity. Increase effect in the Prandtl number gives the increment in thermal conductivity or decrement in viscosity. Due to the low viscosity, the fluid thickness will be reduced, hence the nanoparticle temperature increases with increase of Prandtl number. The same behaviour is observed through Figure 4(c). Figure 4(d) shows the

changes in temperature, as the radiation parameter *Rn* increases the temperature decreases.

Figure 5 is plotted to observe the effects of thermophoresis parameter *Nt*, Brownian motion parameter *Nb*, Prandtl number *Pr* and radiation parameter *Rn* on the nanoparticle volume fraction $\sigma$ of the nanofluid. As the Brownian motion increases, the collisions the random movement of the particles increases, hence there is an increment in nanoparticle volume fraction with the increment in *Nb* (see Figure 5(a)). Figure 5(b) shows that as thermophoresis parameter *Nt* increases, it induces resistance to the movement of the particles in the base fluid and this causes the reduction of nanoparticle volume fraction. It is clear from Figure 5(c) that the nanoparticle volume fraction decreases with an increment in Prandtl number *Pr* as it can link together the viscosity of fluid with thermal conductivity, which decreases the nanoparticle volume fraction. We observe from Figure 5(d) that the increment of radiation parameter *Rn* increases the nanoparticle volume fraction distribution of the nanofluid.

## 4. Conclusion

In the present paper, we have proposed the effect of Hall currents, MHD and electroosmosis on the flow of tangent hyperbolic nanofluid in a porous microchannel. The effects of Brownian motion and thermophoresis have also been considered. The resulting system of highly non-linear equations has been solved using the bvp4c (numerical) package in MATLAB software. This research has been carried out due to the motivation of many applications of combined effects of nanofluid and electroosmosis such as drug delivery, heat regulations in industrial machinery and microscale energy applications. The summary of the findings is as below:

- The velocity of the nanofluid increases with respect to Darcy number.
- There is a decrease in nanofluid velocity with the increase of Hartmann number.
- Nanoparticle temperature decreases with the increment of radiation parameter.
- Nanoparticle volume fraction decreases with the increment of Prandtl number and thermophoresis parameter.
- The results for the Newtonian fluid model can be captured by setting $n \to 0$.

## Disclosure statement

No potential conflict of interest was reported by the author(s).

## ORCID

*K. Ramesh* http://orcid.org/0000-0003-3329-508X

## References

Alfven, H. 1942. "Existence of Electromagnetic-Hydrodynamic Waves." *Nature* 150 (3805): 405–406.

Bakier, A. 2001. "Thermal Radiation Effect on Mixed Convection from Vertical Surfaces in Saturated Porous Media." *International Communications in Heat and Mass Transfer* 28 (1): 119–126.

Choi, S. U. S., and J. A. Eastman. 1995. *Enhancing Thermal Conductivity of Fluids with Nanoparticles*. Argonne, IL: Argonne National Laboratory.

Darcy, H. 1856. *Les Fontaines Publiques De La Ville De Dijon Exposition Et Application Des Principes Suivre Et Des Formules Employer Dans Les Questions De Distribution D'eau*. Paris: Victor Dalmont.

Das, S. K., S. U. S. Choi, W. Yu, and T. Pradeep. 2007. *Nanofluids: Science and Technology*. Milton Keynes: Lightning Source.

Fensom, D. S., and J. Dainty. 1963. "Electro-Osmosis In Nitella." *Canadian Journal of Botany* 41 (5): 685–691.

Ganesh, N. V., Q. M. Al-Mdallal, and P. Kameswaran. 2019. "Numerical Study of MHD Effective Prandtl Number Boundary Layer Flow of Gamma $Al_2O_3$ Nanofluids Past a Melting Surface." *Case Studies in Thermal Engineering* 13: 100413.

Ganesh, N. V., Q. M. Al-Mdallal, K. Reena, and S. Aman. 2019. "Blasius and Sakiadis Slip Flow of $H_2O$–$C_2H_6O_2$ (50:50) Based Nanoliquid with Different Geometry of Boehmite Alumina Nanoparticles." *Case Studies in Thermal Engineering* 16: 100546.

Ganesh, N. V., A. J. Chamkha, Q. M. Al-Mdallal, and P. Kameswaran. 2018. "Magneto-Marangoni Nano-Boundary Layer Flow of Water and Ethylene Glycol Based Gamma $Al_2O_3$ Nanofluids with Non-Linear Thermal Radiation Effects." *Case Studies in Thermal Engineering* 12: 340–348.

Ganesh, N. V., P. K. Kameswaran, Q. M. Al-Mdallal, A. K. A. Hakeem, and B. Ganga. 2018. "Non-Linear Thermal Radiative Marangoni Boundary Layer Flow of Gamma $Al_2O_3$ Nanofluids Past a Stretching Sheet." *Journal of Nanofluids* 7 (5): 944–950.

Jiang, L., J. Mikkelsen, J. M. Koo, D. Huber, S. Yao, L. Zhang, P. Zhou, J. G. Maveety, R. Prasher, J. G. Santiago, T. W. Kenny, and K. E. Goodson. 2002. "Closed-Loop Electroosmotic Microchannel Cooling System for VLSI Circuits." *IEEE Transactions on Components and Packaging Technologies* 25 (3): 347–355.

Keblinski, P., J. A. Eastman, and D. G. Cahill. 2005. "Nanofluids for Thermal Transport." *Materials Today* 8 (6): 36–44.

Kim, S. J., I. C. Bang, J. Buongiorno, and L. W. Hu. 2007. "Study of Pool Boiling and Critical Heat Flux Enhancement in Nanofluids." *Bulletin of the Polish Academy of Sciences: Technical Sciences* 55: 211–216.

Lee, S., S. U. S. Choi, S. Li, and J. A. Eastman. 1999. "Measuring Thermal Conductivity of Fluids Containing Oxide Nanoparticles." *Journal of Heat Transfer* 121 (2): 280–289.

Li, Y., J. B. Li, and R. Zhang. 2004. "Energy-Absorption Performance of Porous Materials in Sandwich Composites Under Hypervelocity Impact Loading." *Composite Structures* 64 (1): 71–78.

Liu, P., and G.-F. Chen. 2014. *Porous Materials Processing and Applications*. Amsterdam: BH, Butterworth-Heinemann/Elsevier.

Liu, P., and X. Ma. 2006. *Detection Method of Porous Materials*. Beijing: Metallurgical Industry Press.

Mahdi, R. A., H. Mohammed, K. Munisamy, and N. Saeid. 2015. "Review of Convection Heat Transfer and Fluid Flow in Porous Media with Nanofluid." *Renewable and Sustainable Energy Reviews* 41: 715–734.

Naseem, A., A. Shafiq, L. Zhao, and M. Farooq. 2018. "Analytical Investigation of Third Grade Nanofluidic Flow Over a Riga Plate Using Cattaneo–Christov Model." *Results in Physics* 9: 961–969.

Nield, D. A., and A. Bejan. 1999. *Convection in Porous Media*. New York: Springer.

Patel, V., and S. K. Kassegne. 2007. "Electroosmosis and Thermal Effects in Magnetohydrodynamic (MHD) Micropumps Using 3D MHD Equations." *Sensors and Actuators B: Chemical* 122 (1): 42–52.

Porrett, R. Jr. 1816. "Curious Galvanic Experiments." *Annals of Philosophy* 8: 74–76.

Ramesh, K. 2018. "Effects of Viscous Dissipation and Joule Heating on the Couette and Poiseuille Flows of a Jeffrey Fluid with Slip Boundary Conditions." *Propulsion and Power Research* 7 (4): 329–341.

Rasool, G., A. Shafiq, C. M. Khalique, and T. Zhang. 2019. "Magnetohydrodynamic Darcy–Forchheimer Nanofluid Flow Over a Nonlinear Stretching Sheet." *Physica Scripta* 94 (10): 105221.

Rasool, G., A. Shafiq, I. Khan, D. Baleanu, K. S. Nisar, and G. Shahzadi. 2020. "Entropy Generation and Consequences of MHD in Darcy–Forchheimer Nanofluid Flow Bounded by Non-Linearly Stretching Surface." *Symmetry* 12 (4): 652.

Rasool, G.,T. Zhang, A. J. Chamkha, A. Shafiq, I. Tlili, and G. Shahzadi. 2019. "Entropy Generation and Consequences of Binary Chemical Reaction on MHD Darcy–Forchheimer Williamson Nanofluid Flow Over Non-Linearly Stretching Surface." *Entropy* 22 (1): 18.

Shafiq, A., Z. Hammouch, and T. Sindhu. 2017. "Bioconvective MHD Flow of Tangent Hyperbolic Nanofluid with Newtonian Heating." *International Journal of Mechanical Sciences* 133: 759–766.
Shafiq, A., Z. Hammouch, and A. Turab. 2018. "Impact of Radiation in a Stagnation Point Flow of Walters' B Fluid Towards a Riga Plate." *Thermal Science and Engineering Progress* 6: 27–33.
Shafiq, A., S. Jabeen, T. Hayat, and A. Alsaedi. 2017. "Cattaneo–Christov Heat Flux Model For Squeezed Flow of Third Grade Fluid." *Surface Review and Letters* 24 (7): 1750098.
Shafiq, A., I. Khan, G. Rasool, A. Seikh, and E.-S. Sherif. 2019. "Significance of Double Stratification in Stagnation Point Flow of Third-Grade Fluid Towards a Radiative Stretching Cylinder." *Mathematics*7 (11): 1103.
Shafiq, A., I. Khan, G. Rasool, E.-S. M. Sherif, and A. H. Sheikh. 2020. "Influence of Single- and Multi-Wall Carbon Nanotubes on Magnetohydrodynamic Stagnation Point Nanofluid Flow Over Variable Thicker Surface with Concave and Convex Effects." *Mathematics* 8 (1): 104.
Shafiq, A., G. Rasool, and C. M. Khalique. 2020. "Significance of Thermal Slip and Convective Boundary Conditions in Three Dimensional Rotating Darcy–Forchheimer Nanofluid Flow." *Symmetry* 12 (5): 741.
Shafiq, A., and T. Sindhu. 2017. "Statistical Study of Hydromagnetic Boundary Layer Flow of Williamson Fluid Regarding a Radiative Surface." *Results in Physics* 7: 3059–3067.
Shafiq, A., I. Zari, I. Khan, T. S. Khan, A. H. Seikh, and E.-S. M. Sherif. 2020. "Marangoni Driven Boundary Layer Flow of Carbon Nanotubes Toward a Riga Plate." *Frontiers in Physics* 7: 215.
Shafiq, A., I. Zari, G. Rasool, I. Tlili, and T. S. Khan. 2019. "On the MHD Casson Axisymmetric Marangoni Forced Convective Flow of Nanofluids." *Mathematics* 7 (11): 1087.
Shapiro, A. P., and R. F. Probstein. 1993. "Removal of Contaminants From Saturated Clay by Electroosmosis." *Environmental Science & Technology* 27 (2): 283–291.
Sharma, A., D. Tripathi, R. Sharma, and A. Tiwari. 2019. "Analysis of Double Diffusive Convection in Electroosmosis Regulated Peristaltic Transport of Nanofluids." *Physica A: Statistical Mechanics and Its Applications* 535: 122148.
Sheikholeslami, M., D. D. Ganji, M. Y. Javed, and R. Ellahi. 2015. "Effect of Thermal Radiation on Magnetohydrodynamics Nanofluid Flow and Heat Transfer by Means of Two Phase Model." *Journal of Magnetism and Magnetic Materials* 374: 36–43.
Zahmatkesh, I. 2007. "Influence of Thermal Radiation on Free Convection Inside a Porous Enclosure." *Emirates Journal for Engineering Research* 12: 47–52.
Zhang, C., L. Zheng, X. Zhang, and G. Chen. 2015. "MHD Flow and Radiation Heat Transfer of Nanofluids in Porous Media with Variable Surface Heat Flux and Chemical Reaction." *Applied Mathematical Modelling* 39 (1): 165–181.

## Appendix

This section aims to give an insight on the numerical formulation and defining the equations in a format understandable to the solver. Bvp4c is a MATLAB solver that deals with solving ordinary differential equations with boundary conditions. The equations are converted in such a manner that the highest order is defined in the form of its subsequent lower order differential terms. Under the aforesaid theory, the governing equations can be written as

$$u'' = \frac{1}{(1-n)+\sqrt{2}nW_e u'}\left(\left(\frac{M^2}{1+m^2}+\frac{1}{Da}\right)u - \kappa^2 U_{HS}\left(\left(\frac{\xi_1+\xi_2}{2\cosh(\kappa)}\right)(\cosh(\kappa y)) - \left(\frac{\xi_1-\xi_2}{2\sinh(\kappa)}\right)(\sinh(\kappa y))\right) - G\right), \tag{A1}$$

$$\theta'' = -\frac{1}{1+RnPr}\left(NbPr\left(\frac{\mathrm{d}\sigma}{\mathrm{d}y}\frac{\mathrm{d}\theta}{\mathrm{d}y}\right) + NtPr\left(\frac{\mathrm{d}\theta}{\mathrm{d}y}\right)^2\right), \tag{A2}$$

$$\sigma'' = -\frac{Nt}{Nb}\theta'', \tag{A3}$$

with the applied boundary value conditions

$$u(-1) = 0, \quad \theta(-1) = 0 \quad \text{and} \quad \sigma(-1) = 0, \tag{A4}$$

$$u(1) = 1, \quad \theta(1) = 1 \quad \text{and} \quad \sigma(1) = 1. \tag{A5}$$

These functions must return the column vectors with the components of $f$ corresponding to the original variables as $f(1) = u$, $f(2) = u'$, $f(3) = u''$, $f(4) = \theta$, $f(5) = \theta'$, $f(6) = \theta''$, $f(7) = \sigma$, $f(8) = \sigma'$, $f(9) = \sigma''$. These functions can be coded in MATLAB as

```
function rhs = rhs_bvp(x, f)
f(3) = ((M^2/(1 + m^2) + 1/Da) * f(1) - G-
κ^2 * U_HS * ((ξ1 + ξ2)/(2 * cosh(κ)) * cosh(κ * x) - (ξ1 - ξ2)/(2 * sinh(κ))
 * sinh(κ * x)))
/((1 - n) + √2 * n * W_e * f(2));
f(6) = -Pr * (Nb * f(5) * f(8) + Nt * (f(5)^2))/(1 + Rn * Pr);
f(9) = -(Nt/Nb) * f(6);
rhs = [f(2)
f(3)
f(5)
f(6)
f(8)
f(9)]
end
function bc = bc_bvp(fa, fb)
bc = [fa(1)
fa(4)
fa(7)
fb(1) - 1
fb(4) - 1
fb(7) - 1]
end
```

Initiating bvp4c requires to provide the mesh size between the boundary values and the initial guesses. This is given by `init = bvpinit (linspace (-1,1),[0 0 0 0 0 0])`. The required solution structure can be expressed as (`sol.x,sol.f`) to obtain the required results of the parameters.